Thermally Stable Passivation towards High Efficiency Inverted Perovskite Solar Cells

Robert D. J. Oliver, Yen-Hung Lin, Alexander J. Horn, Chelsea Q. Xia, Jonathan H. Warby, Michael B. Johnston, Alexandra J. Ramadan, Henry J. Snaith**

Department of Physics, University of Oxford, Clarendon Laboratory, Parks Road, Oxford, OX1 3PU, UK

* Alexandra.ramadan@physics.ox.ac.uk

* henry.snaith@physics.ox.ac.uk

ABSTRACT

Although metal halide perovskite photovoltaics have shown an unprecedented rise in power conversion efficiency (PCE) they remain far from their theoretical PCE limit. Among the highest efficiencies to-date are delivered when polycrystalline films are enhanced via "molecular passivation", but this can introduce new instabilities, in particular under severe accelerated aging conditions (e.g. at 85 °Cn the dark or under full spectrum simulated sunlight). Here, we utilize a benzylammonium bromide passivation treatment to improve device performance, achieving champion stabilized power output (SPO) of 19.5 % in a *p-i-n* device architecture. We correlate the improved device performance with a significant increase in charge carrier diffusion lengths, mobilities and lifetimes. Furthermore, treated devices maintain an increased performance during 120 hours combined stressing under simulated full spectrum sunlight at 85 ºC, indicating that enhancement from this passivation treatment is sustained under harsh accelerated ageing conditions. This is a crucial step towards real-world-operation relevant passivation treatments.

TOC GRAPHIC

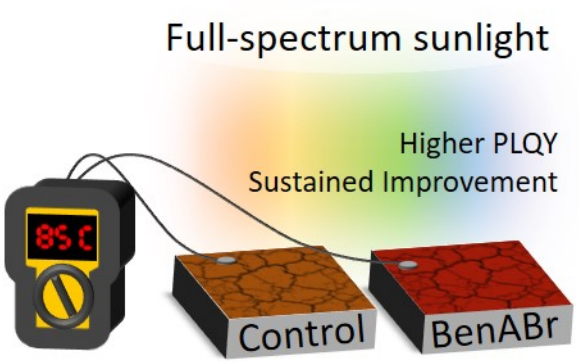

Perovskite solar cells (PSCs) are attracting immense interest in the photovoltaic research community due to their remarkable optoelectronic properties including long carrier diffusion lengths, direct tunable bandgap and high absorption coefficients.[1–4] This has pushed the power conversion efficiencies (PCEs) of laboratory scale single junction PSCs to > 25 %, comparable with established technologies such as c-Si.[5] Many of the fabrication routes which have been reported in the literature to result in high-efficiency PSCs, negatively impact the long-term operational stability of the devices. Notably, the highest efficiency devices still use a substantial amount of methylammonium (MA) as the A-cation, the instability of which is well documented.[6–9] Furthermore, these PSCs employ a *n-i-p* architecture, using 2,2',7,7'-Tetrakis[N,N-di(4-methoxyphenyl)amino]-9,9'-spirobifluorene (Spiro-OMeTAD) as the hole transporting material. Not only is spiro-OMeTAD itself unstable, but the additives required for optimal device performance (lithium-TFSi (Lithium bis(trifluoromethanesulphonyl)imide) and *t*BP (4-tert-Butylpyridine)) further limit the lifetime of the devices substantially.[10,11] As such there has been a significant move within the field towards using the "inverted" *p-i-n* device architecture, which removes the need for spiro-OMeTAD, reduces the hysteresis of PSCs and is more directly applicable to perovskite-on-silicon tandem technologies.[12] However, inverted PSCs have thus far delivered reduced efficiency as compared to their *n-i-p* counterparts, due to lower open-circuit voltages (V_{oc}s) originating from increased non-radiative recombination.[13,14]

Recent work by Jiang *et al.* highlights the limitations of contemporary passivation methods.[15] They report the use of phenethylammonium iodide (PEAI) as a surface passivation treatment in *n-i-p* PSCs and achieve an impressive champion PCE of 23.6 %. However, for thermal aging at 85 °C in the dark, the authors find that they need to replace spiro-OMeTAD with the more thermally stable poly[bis(4-phenyl)(2,4,6-trimethylphenyl)amine] (PTAA), reducing the maximum PCE to

19.1 %. Moreover, the comparative improvement due to the PEAI surface passivation treatment vanishes after less than 50 hours of 85 ˚C aging in the dark. The evidence is that at higher annealing temperatures the PEAI forms a layered 2D phase with PbI_2 from the perovskite, which is assumed to diminish the availability of PEAI to act as a surface passivation molecule.[15] Despite achieving impressive PCEs, this work highlights the need for thermally stable passivation treatments combined with thermally stable device architectures, so that the improvements would last over the lifetime of modules should they be implemented in the field.

Benzylamine rather than the ammonium salt, has been previously used to modify the surface of metal halide perovskites.[16,17] Here we report the use of benzylammonium bromide as a passivation treatment in inverted PSCs. We achieve devices with high champion stabilized power output (SPO) efficiencies of 19.5 % and we show that upon severe accelerated aging at 85 °C, at 0.76 solar irradiance, we observe a sustained improvement from the passivation treatment. This indicates that the passivation treatment does not noticeably deteriorate even under these harsh conditions.

Our study focusses on the effect of BenABr on the triple cation perovskite $Cs_{0.05}(FA_{0.83}MA_{0.17})_{0.95}Pb(I_{0.9}Br_{0.1})_3$ (FA is formamidinium), first reported by Saliba *et al.*, with and without our passivation treatment.[18] To determine the efficacy of BenABr as a passivation treatment we studied its influence on the photoluminescence (PL) of the perovskite films, as well as the charge carrier dynamics. We measured the photoluminescence quantum yield (PLQY) of the perovskite films on glass substrates and on device relevant substrates with isolated charge transport layers (CTLs) following the procedure of De Mello *et al.*[19]. For the hole transport layer (HTL), we use fluorine doped tin oxide (FTO)/ poly(4-butyl-N,N-diphenylaniline) (poly-TPD) substrates, whereas to investigate the PL quenching induced by the electron transport layer (ETL),

perovskite films were first prepared on glass and subsequently coated with PCBM ([6,6]-phenyl-C61-butyric acid methyl ester). PLQY is a powerful technique when assessing the quality of the perovskite semiconductor to be used in a solar cell since an increase in PLQY indicates that less non-radiative recombination is occurring within the film or at the interfaces. A higher PLQY results in an increase in the quasi-Fermi level splitting (QFLS), and should lead to improved device performance through an increase in open-circuit voltage.[20–23] For a standard PV material, the change in QFLS following passivation ($\Delta QFLS = QFLS_{\text{passivated}} - QFLS_{\text{pristine}}$) is given by (further details provided in **Supporting Note 1**),

$$\Delta QFLS = 25.7\ \text{meV} \times \ln\left(\frac{PLQY_{\text{passivated}}}{PLQY_{\text{pristine}}}\right). \qquad (1)$$

Equation 1 is a straightforward way to calculate the expected increase in open-circuit voltage for a given PLQY ratio. Therefore we expect in the region of 60 mV increase in open-circuit voltage, for every order of magnitude increase in radiative efficiency in the complete device.[24] Indeed, **Equation 1** can be modified to calculate the bandgap independent loss from the radiative limit. By setting $PLQY_{\text{passivated}}$ to be unity, i.e. in the ideal case, and then inputting the measured PLQY ($PLQY_{\text{measured}}$), we obtain

$$\Delta QFLS_{\text{rad}} = -25.7\ \text{meV} \times \ln\left(PLQY_{\text{measured}}\right), \qquad (2)$$

where $PLQY_{\text{measured}}$ is expressed in absolute terms.

We present the PLQY values in **Figure 1a** and summarize them in **Table 1**. We determine that the PLQY for the treated films increases in all cases, with the most substantial increase present for the perovskite films coated with PCBM. This PCBM/perovskite interface is known to induce the most non-radiative recombination in *p-i-n* devices, thus the main factor that limiting the open-circuit voltage,[22] corroborated by the lower absolute PLQY which we determine here. The PL spectra are presented in **Figure S1.**

Contact	**PLQY$_{pristine}$ (%)**	***ΔQFLS*$_{rad}$ Pristine (meV)**	**PLQY$_{passivated}$ (%)**	***ΔQFLS*$_{rad}$ Passivated (meV)**	***ΔQFLS* (meV)**
Glass	0.83	123	1.41	109	13.6
polyTPD	0.24	155	0.58	132	22.7
PCBM	0.06	191	0.16	165	25.2

Table 1. PLQY values for pristine and passivated samples processed on glass (glass), with the additional coating of PCBM (PCBM) and processed on polyTPD coated FTO (polyTPD). Also shown are the *ΔQFLS* from the radiative limit *ΔQFLS*$_{rad}$ and the *ΔQFLS* between the passivated and non-passivated films.

The PLQY is nearly 3 times larger for treated films at the n-type interface, with the expected gain of *ΔQFLS* = 25 meV, as we show in the inset in **Figure 1a** and in **Table 1**. Since this interface is the dominant source of non-radiative recombination in *p-i-n* cells, we expect this to translate into a similar boost in V_{oc} in complete devices.[22]

We measured the charge carrier lifetimes of the treated and pristine perovskite thin films on quartz substrates using time-resolved photoluminescence (TRPL) spectroscopy. As can be seen in **Figure 1b**, the PL decay for the treated film is much slower than that of the pristine one. This suggests extended charge carrier lifetimes in the passivated films. From fitting these decays to a stretched exponential (full details given in **Supporting Note 2**), we extract a lifetime of 390 ns and 85 ns for the treated and pristine films respectively. This indicates a reduced level of non-radiative recombination in the treated perovskite, which is typical of reduced trap-state density.

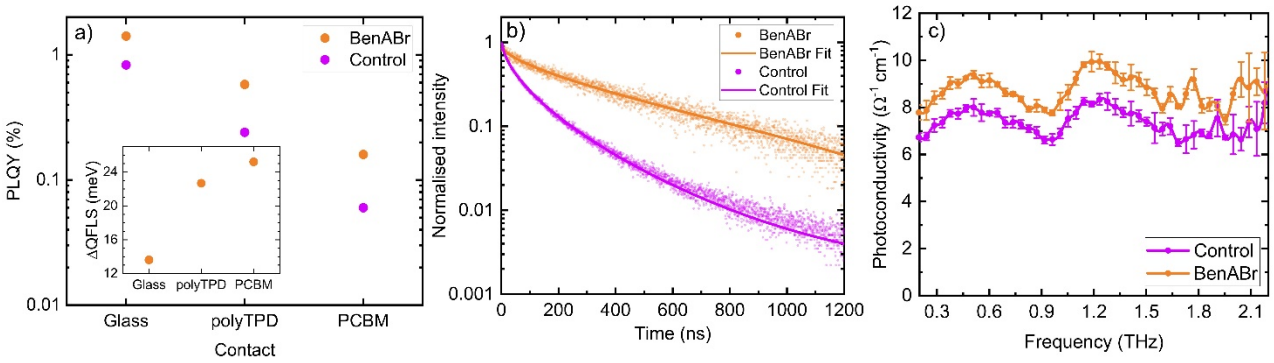

Figure 1. a) PLQY values for treated (orange) and pristine (purple) samples with no charge transport layer (glass), and with isolated p-type (polyTPD) and n-type (PCBM) contacts. *Inset:* The boost in QFLS as determined by **Equation 1** for the same samples. b) Time resolved photoluminescence (TRPL) spectra for pristine (purple) and treated (orange) films. The decays were fitted with a stretched exponential from which lifetimes of 85 ns and 390 ns were extracted for the pristine and treated films respectively. c) Real part of THz photoconductivity spectra induced by photoexcitation. Full spectra with and without photoexcitation including both real and imaginary parts are given in **Figure S2 and S4** in the Supporting Information.

To delve into the short-range charge-carrier dynamics, we performed optical-pump-terahertz-probe spectroscopy (OPTPS) and terahertz time-domain spectroscopy (THz-TDS) on these isolated perovskite films. This non-contact technique enables us to investigate the electro-optic properties, such as photoconductivity and charge-carrier mobility, on a much faster time scale than the PL dynamics, which can be less than 100 fs, and in addition removes the effect of metallic contact incurred on solar cell devices.[2,25,26] **Figure S2** shows the dark conductivity spectra for pristine and treated films, which indicates two prominent phonon modes around 1 THz and 2 THz featured as Lorentzian oscillators. From these data we can calculate the absorption coefficient at THz frequencies, full details are provided in **Supporting Note 3.** The calculated absorption

coefficient is shown in **Figure S3**, and is on the order of 10^3 cm^{-1}, indicating an absorption depth of a few micrometers. The absorption coefficient for the treated film is slightly higher and the two phonon modes are prominent throughout.

We define the photoconductivity as the change of conductivity between a sample under photoexcitation and in the dark. The photoexcitation was applied by an ultrafast laser pulse of 400 nm center wavelength and 5.2 μJcm^{-2} fluence. **Figure 1c** displays the real part of the photoconductivity of the BenABr treated and untreated films, with the imaginary parts shown in **Figure S4**. For both films, the spectrum is relatively flat over the frequency range of the experiment, and agrees with a Drude picture of band-like transport.[27] Small replica of the two phonon modes observed in **Figure S2** can also be seen superimposed on the spectra, indicating an electron-phonon coupling effect, which may suppress the charge-carrier transport.[28] Significantly, the BenABr treated film exhibited a 20 % higher photoconductivity than the pristine film. This additional boost from ~7 $S \cdot cm^{-1}$ to ~9 $S \cdot cm^{-1}$ indicates improved charge carrier mobility in the treated films. We present the photoinduced THz transients in **Figure S5** for completeness.

From fitting the photoconductivity data with a Drude model, details provided in **Supporting Note 4**, we can extract the charge carrier mobilities of the films. The mobilities of the pristine and treated films were $\mu = (51.2 \pm 3.7)$ $cm^2 \cdot V^{-1}s^{-1}$ and $\mu = (62.5 \pm 4.2)$ $cm^2 \cdot V^{-1}s^{-1}$ respectively. As far as we are aware, these mobilities determined from THz spectroscopy are the highest yet reported for polycrystalline metal halide perovskite films, even those reported thus far for the neat iodide perovskites, with typical values ranging from 8-35 $cm^2 \cdot V^{-1}s^{-1}$. This is therefore indicative of extremely high quality of perovskite absorber layers, with much reduced short-range charge carrier scattering. [2,25,29]

From these data we can extract the diffusion length of charge carriers in the perovskite bulk according to the procedure outline in **Supporting Note 5**. Using **Equation S11,** we calculate diffusion lengths of L_d = (2.1 ± 0.2) μm and L_d = (6.1 ± 0.4) μm for reference and treated films respectively. These diffusion lengths are extremely high and thus are promising for high device performance. Further discussion can be found in **Supporting Note 6.**

These improvements in PLQY and charge-carrier lifetimes suggest passivation of trap states. Previous reports on benzylamine suggested that the molecule acts as a passivation agent by anchoring to the to the lead-halide octahedra.[30] To investigate the nature of the chemical binding of the BenABr salt with the perovskite we used X-ray photoemission spectroscopy (XPS). In **Figure 2a** we show high-resolution XPS spectra for the Br 3*d*, Pb 4*f*, Cs 3*d*, I 3*d* core levels in a pristine film and one treated with 5 mg·mL^{-1} of BenABr. We choose this concentration since it resulted in the best device performance, as can be seen in **Figure S6**. Full details of peak positions and fittings can be found in **Figure S7 and S8**. We observe no significant shifts in binding energy of the Br 3*d*, Pb 4*f*, Cs 3*d* and I 3*d* core levels and the peak shape remains unchanged between the pristine samples and those with BenABr present. The binding energies of these peaks show no significant shifts from those reported for similar perovskites.[31,32] Therefore, this lack of difference in the electronic structure of Pb 4*f* between the pristine and treated films does not present evidence that BenABr is binding to the Pb-octahedra within the perovskite, in contrast to what has been suggested with similar molecules.[15,33] It may be the case that the differences in electronic structure of the Pb 4*f* probed within the first ~ 10 nm of the film, are too small to detect when only a surface layer of benzylammonium ions are present on the film. However, we also note that although it is regularly assumed, clear irrefutable evidence is yet to be presented that the post treatment of a 3D

perovskite with larger ammonium cations will automatically result in binding of those larger cations within the lead-halide octahedral frameworks.

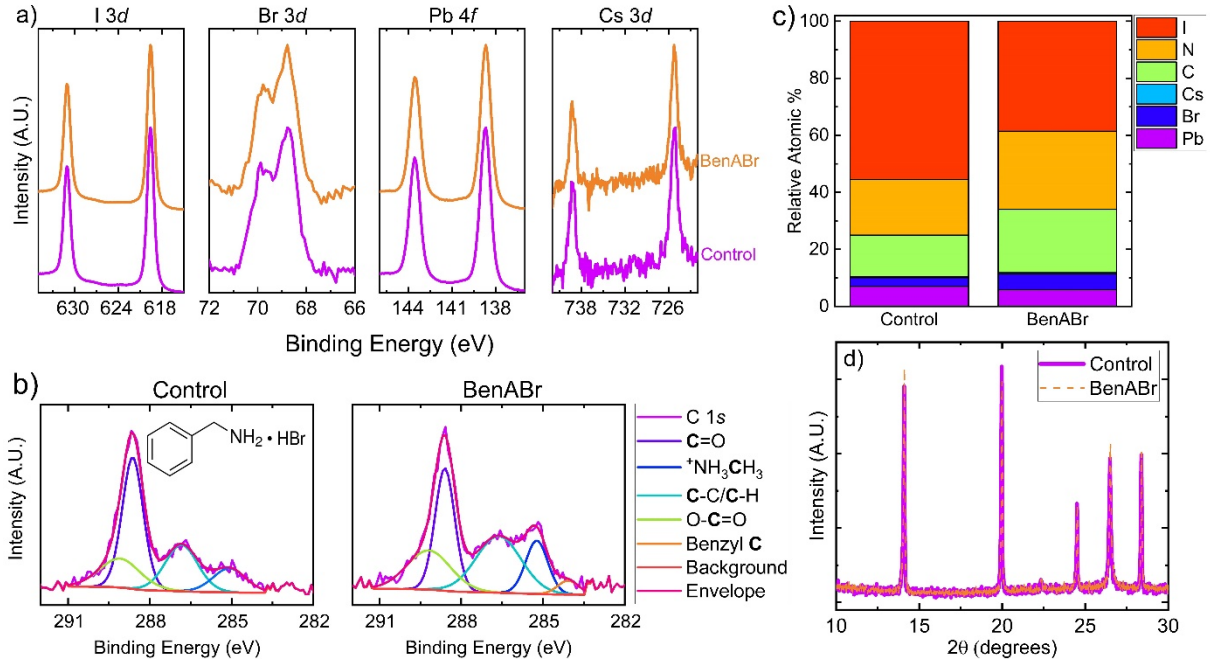

Figure 2. a) High resolution XPS spectra of the Br 3*d*, Pb 4*f*, Cs 3*d*, I 3*d* core levels for pristine (purple) and BenABr treated (orange) films. Full details of the fittings can be found in **Table S1** and **Figure S7 and S8** in the Supporting Information. b) High resolution XPS of the C 1*s* core level for pristine (left) and BenABr treated (right) films with fittings displayed. Inset shows the molecular structure of the BenABr molecule. c) Relative atomic composition of the surface for pristine (left) and BenABr treated (right) films. d) XRD patterns for pristine (purple) and BenABr treated (orange) films. Full XRD patterns are presented **Figure S9** in the Supporting Information.

In contrast to the Pb 4*f* spectra, we do observe significant differences in the C 1*s* spectra, which we show in **Figure 2b**. Of particular note is the peak at 284.1 eV which is present only in the spectra of samples treated with BenABr. We attribute this to the presence of C in an aryl

environment.[34] Additionally using the XPS measurements, we calculated the relative atomic composition of the surface of the perovskite for the pristine and treated films. Our XPS measurements were carried out using a lab-based Al Kα X-ray source which has a penetration depth of up to 10 nm and therefore we can use them to approximate the surface chemistry of the thin film samples. We observe an increase in the relative quantities of C, N and Br on the treated film as compared to the control. This strongly suggests that the BenABr is present predominantly on the surface of the perovskite thin film, but we cannot conclude if there is strong chemical bonding of the benzylammonium to the perovskite structure.

To examine if the treatment with BenABr has a significant influence upon the crystal structure of the underlying perovskite films, we carried out X-ray diffraction (XRD) measurements. The diffraction pattern for treated perovskite films, which we display in **Figure 2d**, exhibits no significant differences when compared to that of pristine perovskite films. Unlike previous reports on similar molecules[15,33,35] we see no evidence for the formation of a two dimensional $BenA_2PbX_4$ phase, where peaks at approximately $2\theta = 12°$, 18° and 25° would be expected.[36] Therefore we conclude that BenABr does not influence the crystal structure of the perovskite films. For completeness, we carried out scanning electron microscopy (SEM) to examine the morphology of the respective systems**.** The BenABr treated films exhibit morphologies akin to the pristine films, which we present in **Figure S10**. We note that an undetectably small 2D phase could have formed on the surface of the perovskite, but our structural, chemical, and electronic characterization has demonstrated no evidence for this. Therefore, our materials characterization suggests that whilst BenABr improves the optoelectronic properties of the perovskite film, it does this without influencing the chemical or structural properties of the material suggesting that it is acting as a defect/trap passivation agent. We suggest that the passivation mechanism may be due to the filling

of halide vacancies on the surface of the perovskite, as evidenced by a greater fraction of bromide in the elemental composition shown in **Figure 2c.**

In order to assess the impact of BenABr passivation in complete solar cells, we fabricated a series of PSCs with the concentrations of BenABr ranging from 3 – 6 mg·mL^{-1} in the following device architecture: FTO/Poly-TPD/perovskite/PCBM/BCP (bathocuproine) /Ag. We observed a significant increase in performance for the BenABr-treated devices, as compared to the untreated devices. We found an optimum concentration of BenABr at 5 mg·mL^{-1}, and show the full range of BenABr concentrations investigated and their relevant device parameters in **Figure S6**. We present champion and average device parameters in **Table 2**, as well as a histogram showing the PCEs for the reference samples and those with the optimal concentration of the treatment in **Figure S11**.

Condition	**PCE (%)**	**V_{oc} (V)**	**J_{sc} (mAcm^{-2})**	**Fill Factor (%)**
Control	15.09 (18.17)	1.038 (1.06)	20.38 (22.72)	72.0 (76.7)
3 mg·mL^{-1}	15.86 (18.57)	1.042 (1.06)	21.39 (22.66)	71.9 (78.6)
4 mg·mL^{-1}	16.42 (18.48)	1.055 (1.06)	20.82 (21.72)	75.3 (80.5)
5 mg·mL^{-1}	16.75 (19.28)	1.061 (1.08)	21.02 (22.77)	75.9 (79.9)
6 mg·mL^{-1}	15.84 (17.59)	1.046 (1.06)	20.43 (21.35)	74.6 (77.8)

Table 2. Average (champion) device parameters for the BenABr concentrations investigated.

In **Figure 3a** we show the champion stabilized power output (SPO) for control and 5 mg·mL^{-1} treated devices. We observe a significant improvement, achieving an impressive SPO of 19.5 % in the treated devices, as compared to 18.4 % for control devices. The BenABr treatment also reduced the hysteresis in the *JV* scans, which is evident from the champion *JV* curves presented in **Figure S12**. We note that the BenABr treatment ameliorates all of the main device parameters.

For the optimal concentration of 5 mg·mL^{-1}, the fill factor increases by 3.8 % absolute, and there is an increase in the open-circuit voltage of 22 mV, consistent with reduced non-radiative recombination. Further, this improvement in V_{oc} is entirely consistent with the increased luminescence efficiency of the perovskite films with p- or n-type contacts (**Figure 1a**), from which we predict an increase in quasi-Fermi level splitting of ~ 25 mV.

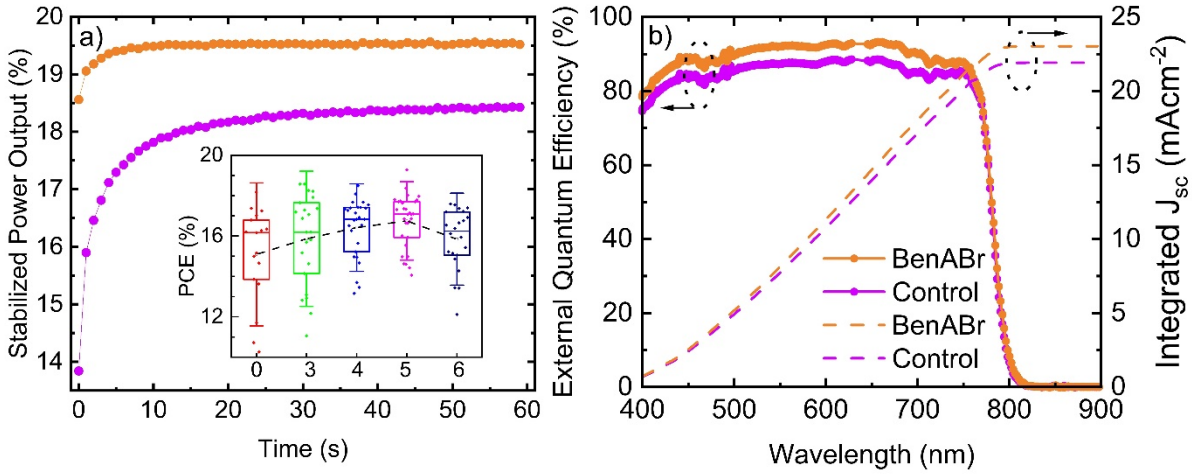

Figure 3. a) Stabilized power output (SPO) traces for the champion control (purple) and treated (orange) devices. *JV* curves of the same devices are shown in **Figure S12**. *Inset:* Box plots showing the PCE for the range of BenABr concentrations investigated (x-axis unit is in mg/mL) The dotted line is a guide for the eye and connects the mean value of the distributions. The corresponding box plots for the other device parameters may be found in **Figure S6**. b) External quantum efficiency (EQE) spectra for champion control (purple) treated (orange) devices. Integrating the EQE over the AM 1.5 spectrum gives J_{sc} values of 21.9 mAcm^{-2} and 23.0 mAcm^{-2} for control and treated devices respectively.

Another route in which the BenABr treatment leads to improved device performance is through an increased short-circuit current density. To verify this, we measured the external quantum

efficiency (EQE) of our devices. As can be seen in **Figure 3b**, there is a panchromatic increase of the EQE with the BenABr treatment. These data suggest improved charge extraction to the external circuit across the entire range of our absorption, which leads to higher short-circuit current densities. Integrating the EQE for control and treated devices over the AM 1.5 solar spectrum gives short-circuit current density values of 21.9 $mAcm^{-2}$ and 23.0 $mAcm^{-2}$ respectively (an error of < 3 % compared with the *JV* scans).

This enhancement of the short circuit current density following the BenABr treatment is unexpected. The diffusion lengths of charge carriers, as judged from our mobility and carrier lifetime measurements, is substantial for both control and treated films, at 2.1 and 6.1 μm respectively. While these values are upper bounds, as they don't account for reduced lifetimes due to interfacial recombination induced by the charge transport layers, the high fill factors which we observe for both cases are also consistent with diffusion current (as opposed to drift) being responsible for charge transport out of the absorber layer, demonstrating that a strong electric field (as is present under short-circuit conditions) is not required to extract charge carriers. We therefore postulate that the improvement in J_{sc} with BenABr treatment may be due to increased homogeneity with the BenABr treatment. In the reference cells, there may be complete polycrystalline domains which are not contributing to photocurrent generation and collection, which would reduce the J_{sc} while leaving the FF largely unaffected, if these domains are not in communication with the rest of the film. Heterogeneity is well known to be present in PSCs[37] , but its influence on the J_{sc} is not yet fully understood. Understanding the precise origin of this increased photocurrent density is beyond the scope of the present work but is the subject of ongoing investigations. Thermal stability is an essential requirement for surface passivation treatments, otherwise any improvement due to the passivation would be lost over time. Therefore,

we investigated the stability of PSCs with the BenABr treatment by stressing encapsulated devices at elevated (85 ºC) temperatures under simulated solar irradiance concomitantly, in an open-circuit condition. This is condition ISOS-L-2 as set out by the stability consensus, and we choose the higher temperature (85 ºC instead of 65 ºC) and open-circuit conditions.[38]

We employed the relatively harsh 85 ˚C light soaking (AM 1.5) aging conditions since we are interested in understanding if the improvement owing to the BenABr treatment itself is maintained under these conditions, rather than assessing the overall stability of the underlying perovskite. We present the evolution of the PV performance parameters in **Figure 4**. Both treated and reference devices decay relatively rapidly under these severe aging conditions. However, this is consistent with what we have recently reported for similar control devices, without any further improvement with ionic stabilizing additives.[39]

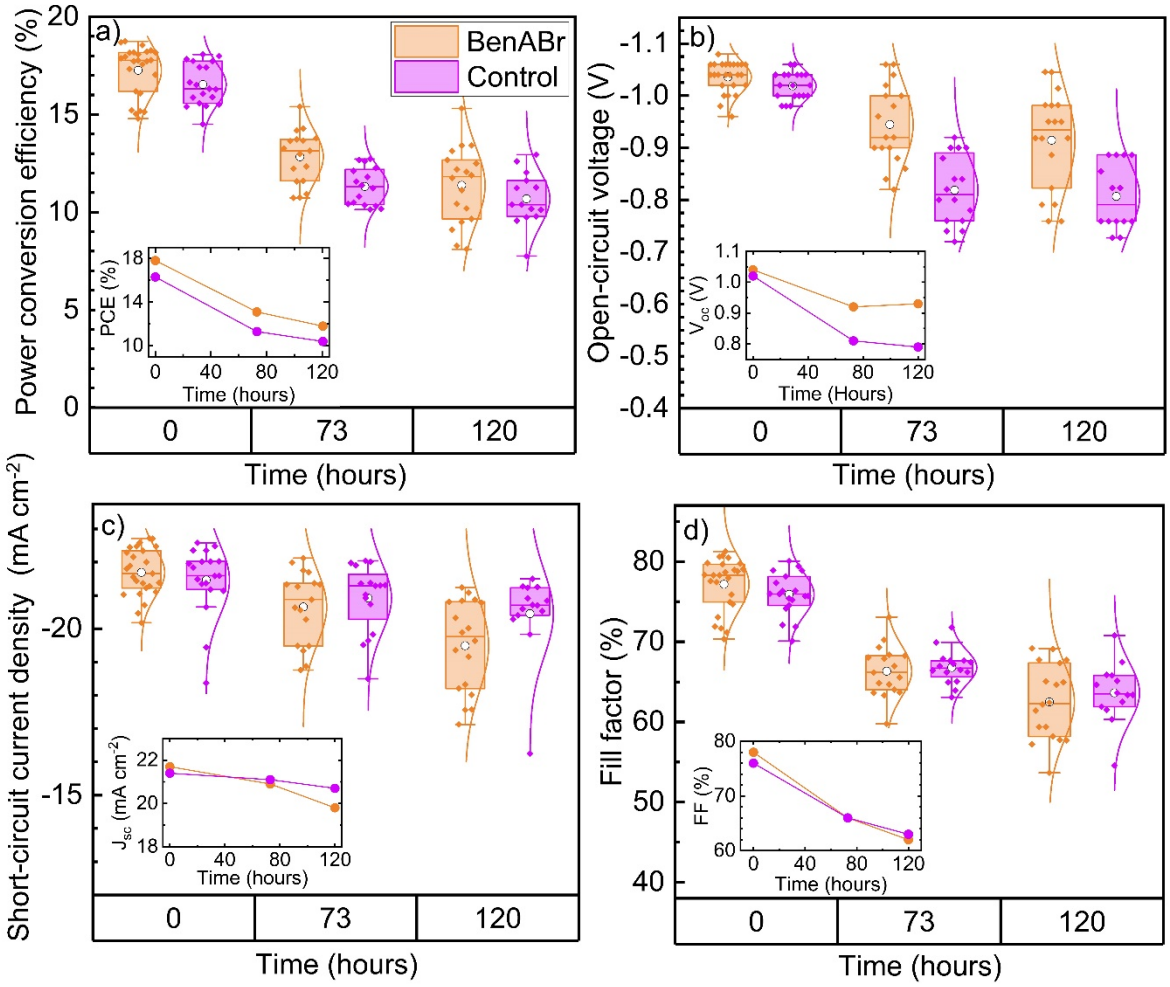

Figure 4. Evolution of the a) PCE, b) V_{oc}, c) J_{sc} and d) fill factor for encapsulated treated (orange) and control (purple) devices aged at 85 ºC under simulated AM 1.5 irradiance in an open-circuit condition (as per ISOS-L-2[38]). The data points are overlapped onto the boxplots which show the median (central line), the mean (white circle), the median of the upper and lower halves of the data (top and bottom lines of the box respectively). The top and bottom whiskers are drawn to the highest/lowest datapoint within 1.5 times the interquartile range from the top and bottom of the box respectively. Normal distributions to the data are shown on the right of each box plot. The insets show the evolution of the median values of each device parameter over time.

Importantly, we find here that the devices treated with BenABr maintain an increased performance over their pristine counterparts, most evident in the inset on **Figure 4a.** This suggests that the improvement from the passivation treatment is maintained under light and high temperature thermal stressing. On further investigation, we see that the BenABr treatment maintains a substantial improvement in the open circuit voltage, from a boost of ~20 mV to 140 mV. This indicates a significantly reduced level of non-radiative recombination in the treated devices during the ageing experiment suggesting that BenABr is continuing to act as a passivation treatment during the aging and has not degraded and lost functionality. This is notably in contrast to other contemporary passivation routes, such as phenethylammonium iodide.[15]

In this work we have demonstrated a thermally stable passivation treatment, which is an essential requirement if any treatment is to have a prospect of being implemented in modules intended for use in the field. The treatment, benzylammonium bromide, increases the optoelectronic quality of the perovskite semiconductor layer as assessed through photoluminescence and time domain THz spectroscopic studies. This improvement occurs despite there being no evidence for the BenABr treatment chemically binding to the perovskite, or changing its crystallinity or surface morphology. The work we have presented here is an important step forward on the road to the commercialization of PSCs, since we highlight the potential for thermally stable passivation treatments resulting in high efficiency devices.

AUTHOR INFORMATION

Corresponding author email addresses: alexandra.ramadan@physics.ox.ac.uk, henry.snaith@physics.ox.ac.uk

Group website: https://www2.physics.ox.ac.uk/research/photovoltaic-and-optoelectronic-device-group

Twitter handle: @SnaithGroup

Notes

Henry Snaith is co-founder and Chief Scientific Officer of Oxford PV, a company commercializing perovskite photovoltaics.

ACKNOWLEDGMENT

The authors would like to thank the EPSRC (Engineering and Physics Sciences Research Council) for financial support. RDJO would like to express his gratitude to the Penrose Scholarship for his funding his studentship. The authors are grateful to Suhas Mahesh for insightful discussions.

Supporting Information available:

Details of device fabrication and experimental procedures can be found in the Supporting Information. Additional data pertaining to the THz spectroscopy measurements, XPS measurements and fitting, device performance as well as x-ray diffraction and SEM images are also available. Deeper discussion on the calculation of the QFLS, absorption coefficient, TRPL

fitting, Drude fit and diffusion length calculation and charge carrier transport discussion are also presented.

REFERENCES

(1) Stranks, S. D.; Eperon, G. E.; Grancini, G.; Menelaou, C.; Alcocer, M. J. P.; Leijtens, T.; Herz, L. M.; Petrozza, A.; Snaith, H. J. Electron-Hole Diffusion Lengths Exceeding 1 Micrometer in an Organometal Trihalide Perovskite Absorber. *Science (80-.).* **2013**, *342* (6156), 341–344. https://doi.org/10.1126/science.1243982.

(2) Wehrenfennig, C.; Eperon, G. E.; Johnston, M. B.; Snaith, H. J.; Herz, L. M. High Charge Carrier Mobilities and Lifetimes in Organolead Trihalide Perovskites. *Adv. Mater.* **2014**, *26* (10), 1584–1589. https://doi.org/10.1002/adma.201305172.

(3) McMeekin, D. P.; Sadoughi, G.; Rehman, W.; Eperon, G. E.; Saliba, M.; Hörantner, M. T.; Haghighirad, A.; Sakai, N.; Korte, L.; Rech, B.; Johnston, M. B.; Herz, L. M.; Snaith, H. J. A Mixed-Cation Lead Mixed-Halide Perovskite Absorber for Tandem Solar Cells. *Science (80-.).* **2016**, *351* (6269), 151–155. https://doi.org/10.1126/science.aad5845.

(4) Huang, J.; Yuan, Y.; Shao, Y.; Yan, Y. Understanding the Physical Properties of Hybrid Perovskites for Photovoltaic Applications. *Nat. Rev. Mater.* **2017**, *2*, 1–19. https://doi.org/10.1038/natrevmats.2017.42.

(5) NREL Best Research-Cell Efficiency Chart; Accessed 28 Feb 20.

(6) Conings, B.; Drijkoningen, J.; Gauquelin, N.; Babayigit, A.; D'Haen, J.; D'Olieslaeger, L.;

Ethirajan, A.; Verbeeck, J.; Manca, J.; Mosconi, E.; De Angelis, F.; Boyen, H. G. Intrinsic Thermal Instability of Methylammonium Lead Trihalide Perovskite. *Adv. Energy Mater.* **2015**, *5* (15), 1–8. https://doi.org/10.1002/aenm.201500477.

(7) Habisreutinger, S. N.; McMeekin, D. P.; Snaith, H. J.; Nicholas, R. J. Research Update: Strategies for Improving the Stability of Perovskite Solar Cells. *APL Mater.* **2016**, *4* (9), 091503. https://doi.org/10.1063/1.4961210.

(8) Nenon, D. P.; Christians, J. A.; Wheeler, L. M.; Blackburn, J. L.; Sanehira, E. M.; Dou, B.; Olsen, M. L.; Zhu, K.; Berry, J. J.; Luther, J. M. Structural and Chemical Evolution of Methylammonium Lead Halide Perovskites during Thermal Processing from Solution. *Energy Environ. Sci.* **2016**, *9* (6), 2072–2082. https://doi.org/10.1039/c6ee01047d.

(9) Dualeh, A.; Gao, P.; Seok, S. Il; Nazeeruddin, M. K.; Grätzel, M. Thermal Behavior of Methylammonium Lead-Trihalide Perovskite Photovoltaic Light Harvesters. *Chem. Mater.* **2014**, *26* (21), 6160–6164. https://doi.org/10.1021/cm502468k.

(10) Christians, J. A.; Schulz, P.; Tinkham, J. S.; Schloemer, T. H.; Harvey, S. P.; Tremolet De Villers, B. J.; Sellinger, A.; Berry, J. J.; Luther, J. M. Tailored Interfaces of Unencapsulated Perovskite Solar Cells for >1,000 Hour Operational Stability. *Nat. Energy* **2018**, *3* (1), 68–74. https://doi.org/10.1038/s41560-017-0067-y.

(11) Hou, Y.; Du, X.; Scheiner, S.; McMeekin, D. P.; Wang, Z.; Li, N.; Killian, M. S.; Chen, H.; Richter, M.; Levchuk, I.; Schrenker, N.; Spiecker, E.; Stubhan, T.; Luechinger, N. A.; Hirsch, A.; Schmuki, P.; Steinrück, H. P.; Fink, R. H.; Halik, M.; Snaith, H. J.; Brabec, C. J. A Generic Interface to Reduce the Efficiency-Stability-Cost Gap of Perovskite Solar Cells. *Science (80-.).* **2017**, *358* (6367), 1192–1197.

https://doi.org/10.1126/science.aao5561.

(12) Snaith, H. J.; Abate, A.; Ball, J. M.; Eperon, G. E.; Leijtens, T.; Noel, N. K.; Stranks, S. D.; Wang, J. T. W.; Wojciechowski, K.; Zhang, W. Anomalous Hysteresis in Perovskite Solar Cells. *J. Phys. Chem. Lett.* **2014**, *5* (9), 1511–1515. https://doi.org/10.1021/jz500113x.

(13) Stolterfoht, M.; Wolff, C. M.; Márquez, J. A.; Zhang, S.; Hages, C. J.; Rothhardt, D.; Albrecht, S.; Burn, P. L.; Meredith, P.; Unold, T.; Neher, D. Visualization and Suppression of Interfacial Recombination for High-Efficiency Large-Area Pin Perovskite Solar Cells. *Nat. Energy* **2018**, *3* (10), 847–854. https://doi.org/10.1038/s41560-018-0219-8.

(14) Momblona, C.; Gil-Escrig, L.; Bandiello, E.; Hutter, E. M.; Sessolo, M.; Lederer, K.; Blochwitz-Nimoth, J.; Bolink, H. J. Efficient Vacuum Deposited P-i-n and n-i-p Perovskite Solar Cells Employing Doped Charge Transport Layers. *Energy Environ. Sci.* **2016**, *9* (11), 3456–3463. https://doi.org/10.1039/c6ee02100j.

(15) Jiang, Q.; Zhao, Y.; Zhang, X.; Yang, X.; Chen, Y.; Chu, Z.; Ye, Q.; Li, X.; Yin, Z.; You, J. Surface Passivation of Perovskite Film for Efficient Solar Cells. *Nat. Photonics* **2019**, *13* (7), 460–466. https://doi.org/10.1038/s41566-019-0398-2.

(16) Wang, F.; Geng, W.; Zhou, Y.; Fang, H.; Tong, C.; Loi, M. A.; Liu, L.; Zhao, N. Phenylalkylamine Passivation of Organolead Halide Perovskites Enabling High-Efficiency and Air-Stable Photovoltaic Cells. **2016**, *28* (45), 9986–9992. https://doi.org/10.1002/adma.201603062.

(17) Zhou, Y.; Wang, F.; Cao, Y.; Wang, J. P.; Fang, H. H.; Loi, M. A.; Zhao, N.; Wong, C. P. Benzylamine-Treated Wide-Bandgap Perovskite with High Thermal-Photostability and

Photovoltaic Performance. *Adv. Energy Mater.* **2017**, *7* (22), 4–10. https://doi.org/10.1002/aenm.201701048.

(18) Saliba, M.; Matsui, T.; Seo, J. Y.; Domanski, K.; Correa-Baena, J. P.; Nazeeruddin, M. K.; Zakeeruddin, S. M.; Tress, W.; Abate, A.; Hagfeldt, A.; Grätzel, M. Cesium-Containing Triple Cation Perovskite Solar Cells: Improved Stability, Reproducibility and High Efficiency. *Energy Environ. Sci.* **2016**, *9* (6), 1989–1997. https://doi.org/10.1039/c5ee03874j.

(19) De Mello, J. C.; Wittmann, H. F.; Friend, R. H. An Improved Experimental Determination of External Photoluminescence Quantum Efficiency. *Adv. Mater.* **1997**, *9* (3), 230–232. https://doi.org/10.1002/adma.19970090308.

(20) Ross, R. T. Some Thermodynamics of Photochemical Systems. *J. Chem. Phys.* **1967**, *46* (12), 4590–4593. https://doi.org/10.1063/1.1840606.

(21) Miller, O. D.; Yablonovitch, E.; Kurtz, S. R. Strong Internal and External Luminescence as Solar Cells Approach the Shockley-Queisser Limit. *IEEE J. Photovoltaics* **2012**, *2* (3), 303–311. https://doi.org/10.1109/JPHOTOV.2012.2198434.

(22) Stolterfoht, M.; Caprioglio, P.; Wolff, C. M.; Márquez, J. A.; Nordmann, J.; Zhang, S.; Rothhardt, D.; Hörmann, U.; Amir, Y.; Redinger, A.; Kegelmann, L.; Zu, F.; Albrecht, S.; Koch, N.; Kirchartz, T.; Saliba, M.; Unold, T.; Neher, D. The Impact of Energy Alignment and Interfacial Recombination on the Internal and External Open-Circuit Voltage of Perovskite Solar Cells. *Energy Environ. Sci.* **2019**, *12* (9), 2778–2788. https://doi.org/10.1039/c9ee02020a.

(23) Caprioglio, P.; Stolterfoht, M.; Wolff, C. M.; Unold, T.; Rech, B.; Albrecht, S.; Neher, D. On the Relation between the Open-Circuit Voltage and Quasi-Fermi Level Splitting in Efficient Perovskite Solar Cells. *Adv. Energy Mater.* **2019**, *9* (33), 1901631. https://doi.org/10.1002/aenm.201901631.

(24) Nayak, P. K.; Mahesh, S.; Snaith, H. J.; Cahen, D. Photovoltaic Solar Cell Technologies: Analysing the State of the Art. *Nat. Rev. Mater.* **2019**, *4* (4), 269–285. https://doi.org/10.1038/s41578-019-0097-0.

(25) Milot, R. L.; Eperon, G. E.; Snaith, H. J.; Johnston, M. B.; Herz, L. M. Temperature-Dependent Charge-Carrier Dynamics in CH3NH3PbI3 Perovskite Thin Films. *Adv. Funct. Mater.* **2015**, *25* (39), 6218–6227. https://doi.org/10.1002/adfm.201502340.

(26) Johnston, M. B.; Herz, L. M. Hybrid Perovskites for Photovoltaics: Charge-Carrier Recombination, Diffusion, and Radiative Efficiencies. *Acc. Chem. Res.* **2016**, *49* (1), 146–154. https://doi.org/10.1021/acs.accounts.5b00411.

(27) Milot, R. L.; Klug, M. T.; Davies, C. L.; Wang, Z.; Kraus, H.; Snaith, H. J.; Johnston, M. B.; Herz, L. M. The Effects of Doping Density and Temperature on the Optoelectronic Properties of Formamidinium Tin Triiodide Thin Films. *Adv. Mater.* **2018**, *30* (44), 1804506. https://doi.org/10.1002/adma.201804506.

(28) Wright, A. D.; Verdi, C.; Milot, R. L.; Eperon, G. E.; Pérez-Osorio, M. A.; Snaith, H. J.; Giustino, F.; Johnston, M. B.; Herz, L. M. Electron-Phonon Coupling in Hybrid Lead Halide Perovskites. *Nat. Commun.* **2016**, *7* (1), 11755. https://doi.org/10.1038/ncomms11755.

(29) Herz, L. M. Charge-Carrier Mobilities in Metal Halide Perovskites: Fundamental

Mechanisms and Limits. *ACS Energy Lett.* **2017**, *2* (7), 1539–1548. https://doi.org/10.1021/acsenergylett.7b00276.

(30) Yang, S.; Wang, Y.; Liu, P.; Cheng, Y. B.; Zhao, H. J.; Yang, H. G. Functionalization of Perovskite Thin Films with Moisture-Tolerant Molecules. *Nat. Energy* **2016**, *1* (2), 1–7. https://doi.org/10.1038/NENERGY.2015.16.

(31) Ramadan, A. J.; Noel, N. K.; Fearn, S.; Young, N.; Walker, M.; Rochford, L. A.; Snaith, H. J. Unravelling the Improved Electronic and Structural Properties of Methylammonium Lead Iodide Deposited from Acetonitrile. *Chem. Mater.* **2018**, *30* (21), 7737–7743. https://doi.org/10.1021/acs.chemmater.8b03084.

(32) Ramadan, A. J.; Ralaiarisoa, M.; Zu, F.; Rochford, L. A.; Wenger, B.; Koch, N.; Snaith, H. J. Revealing the Stoichiometric Tolerance of Lead Trihalide Perovskite Thin Films. *Chem. Mater.* **2020**, *32* (1), 114–120. https://doi.org/10.1021/acs.chemmater.9b02639.

(33) Gharibzadeh, S.; Abdollahi Nejand, B.; Jakoby, M.; Abzieher, T.; Hauschild, D.; Moghadamzadeh, S.; Schwenzer, J. A.; Brenner, P.; Schmager, R.; Haghighirad, A. A.; Weinhardt, L.; Lemmer, U.; Richards, B. S.; Howard, I. A.; Paetzold, U. W. Record Open-Circuit Voltage Wide-Bandgap Perovskite Solar Cells Utilizing 2D/3D Perovskite Heterostructure. *Adv. Energy Mater.* **2019**, *9* (21), 1–10. https://doi.org/10.1002/aenm.201803699.

(34) Liu, Z.; Su, Q.; Ju, P.; Li, X.; Li, G.; Wu, Q.; Yang, B. A Hydrophilic Covalent Organic Framework for Photocatalytic Oxidation of Benzylamine in Water. *Chem. Commun.* **2020**, *56* (5), 766–769. https://doi.org/10.1039/c9cc07661a.

(35) Zhou, Y.; Wang, F.; Cao, Y.; Wang, J.; Fang, H.; Loi, M. A. Benzylamine-Treated Wide-Bandgap Perovskite with High Thermal-Photostability and Photovoltaic Performance. **2017**, *1701048*, 4–10. https://doi.org/10.1002/aenm.201701048.

(36) Mao, L.; Tsai, H.; Nie, W.; Ma, L.; Im, J.; Stoumpos, C. C.; Malliakas, C. D.; Hao, F.; Wasielewski, M. R.; Mohite, A. D.; Kanatzidis, M. G. Role of Organic Counterion in Lead- and Tin-Based Two-Dimensional Semiconducting Iodide Perovskites and Application in Planar Solar Cells. *Chem. Mater.* **2016**, *28* (21), 7781–7792. https://doi.org/10.1021/acs.chemmater.6b03054.

(37) DeQuilettes, D. W.; Vorpahl, S. M.; Stranks, S. D.; Nagaoka, H.; Eperon, G. E.; Ziffer, M. E.; Snaith, H. J.; Ginger, D. S. Impact of Microstructure on Local Carrier Lifetime in Perovskite Solar Cells. *Science (80-.).* **2015**, *348* (6235), 683–686. https://doi.org/10.1126/science.aaa5333.

(38) Khenkin, M. V; Katz, E. A.; Abate, A.; Bardizza, G.; Berry, J. J.; Brabec, C.; Brunetti, F.; Bulović, V.; Burlingame, Q.; Carlo, A. Di; Matheron, M.; Mcgehee, M.; Meitzner, R.; Nazeeruddin, M. K. Consensus Statement for Stability Assessment and Reporting for Perovskite Photovoltaics Based on ISOS Procedures. *Nat. Energy* **2020**, *5* (January), 35–49. https://doi.org/10.1038/s41560-019-0529-5.

(39) Lin, Y.-H.; Sakai, N.; Da, P.; Wu, J.; Sansom, H. C.; Ramadan, A. J.; Mahesh, S.; Liu, J.; Oliver, R. D. J.; Lim, J.; Aspitarte, L.; Sharma, K.; Madhu, P. K.; Morales- Vilches, A. B.; Nayak, P. K.; Bai, S.; Gao, F.; Grovenor, C. R. M.; Johnston, M. B.; Labram, J. G.; Durrant, J. R.; Ball, J. M.; Wenger, B.; Stannowski, B.; Snaith, H. J. A Piperidinium Salt Stabilizes Efficient Metal-Halide Perovskite Solar Cells. *Science (80-.).* **2020**, *369* (6499), 96–102.